

First Coincidences in Pre-Clinical Compton Camera Prototype for Medical Imaging

A. Studen^{a,*} D. Burdette^b E. Chesi^b V. Cindro^a
N. H. Clinthorne^c W. Dulinski^d J. Fuster^e L. Han^f
K. Honscheid^b H. Kagan^b C. Lacasta^e G. Llosá^e
A. C. Marques^g N. Malakhov^b D. Meier^h M. Mikuž^a
S. J. Park^f S. Roeⁱ W. L. Rogers^c J. Steinberg^b
P. Weilhammerⁱ S. J. Wilderman^f L. Zhang^f D. Žontar^a

^a*Institute Jožef Stefan and Department of Physics, University of Ljubljana, Ljubljana, Slovenia*

^b*Ohio State University, Physics Department, Columbus, Ohio, U. S. A*

^c*Medical School, University of Michigan, Ann Arbor, Michigan, U. S. A.*

^d*LEPSI, IN2P3/CNRS-ULP, Strasbourg, France*

^e*Inst. de Fisica Corpuscular, CSIC, Universitat de Valencia, Valencia, Spain*

^f*College of Engineering, University of Michigan, Ann Arbor, U. S. A.*

^g*CFNUL, Univ. Lisbon, Lisbon and ITN, Sacavem, Portugal*

^h*Ideas ASA, Oslo, Norway*

ⁱ*CERN, Geneva, Switzerland*

Abstract

Compton collimated imaging may improve the detection of gamma rays emitted by radioisotopes used in single photon emission computed tomography (SPECT). We present a crude prototype consisting of a single 500 μm thick, 256 pad silicon detector with pad size of $1.4 \times 1.4 \text{ mm}^2$, combined with a $15 \times 15 \times 1 \text{ cm}^3$ NaI scintillator crystal coupled to a set of 20 photo multipliers. Emphasis is placed on the performance of the silicon detector and the associated read-out electronics, which has so far proved to be the most challenging part of the set-up. Results were obtained using the VATAGP3, 128 channel low-noise self-triggering ASIC as the silicon detector's front-end. The noise distribution (σ) of the spectroscopic outputs gave an equivalent noise charge (ENC) with a mean value of $\langle\sigma\rangle=137 \text{ e}$ with a spread of 10 e, corresponding to an energy resolution of 1.15 keV FWHM for the scattered electron energy. Threshold settings above 8.2 keV were required for stable operation of the trigger. Coincident Compton scatter events in both modules were observed for photons emitted by ^{57}Co source with principal gamma ray energies of 122 and 136 keV.

Key words: silicon pad detectors, medical imaging, Compton camera.
PACS: 87.58.Ce Single photon emission computed tomography (SPECT),
29.40.Gx Tracking and position-sensitive detectors.

1 Introduction: Compton camera principle

A Compton camera [1], as depicted in figure 1, uses two sets of detectors. In the first detector, the scatterer, the initial photon with energy E_γ is Compton scattered and E_e , the energy of the scattered electron is recorded together with the interaction position. The scattered photon is photo-absorbed in the second detector, the absorber. The interaction points in both detectors yield the scattered photon's direction. The scattering angle θ determining the direction of the initial photon is calculated from E_e using the relation: $\sin(\theta/2) = \sqrt{m_e c^2 E_e / 2E_\gamma (E_\gamma - E_e)}$ with $m_e c^2 = 511$ keV. Hence the position of the photon source can be fixed to a cone surface, with apex at the interaction point in the scatterer, opening angle θ and axis along the secondary photon track. The intersections of several such cones reconstruct the three-dimensional distribution of the γ -ray sources.

This paper describes a prototype for medical imaging with a silicon scatterer and a scintillation camera. Silicon pad detectors with a pitch of 1.4 mm were chosen as a scatterer. They provide the necessary sub-millimeter spatial resolution. The challenge is to obtain the energy resolution of 1 keV FWHM that is needed for improved imaging. We rely on scintillation cameras as absorbers as they are well established, provide adequate position resolution and high stopping power at a modest price and high reliability. A description of both detector modules is presented, followed by the details of the coincidence set-up. In conclusion the planned clinical application aimed at screening of prostate cancer is described.

2 The silicon scatterer module

Figure 2 shows a hybrid with the silicon sensor attached to two read-out chips. The sensor was chosen from a batch designed [2], [3], [4] and processed by SINTEF [5]. It is a 500 μm thick, 256 pad detector with a $\text{p}^+\text{-n-n}^+$ doping profile and pad size of 1.4×1.4 mm². The first metal layer completely covers

* Corresponding author

Email address: Andrej.Studen@ijs.si (A.Studen).

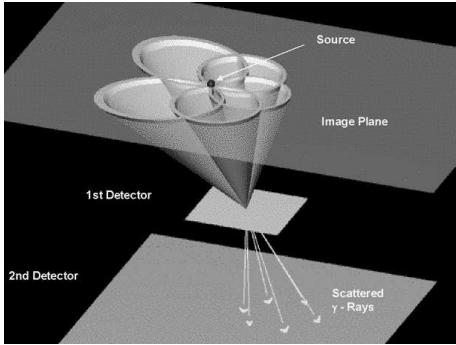


Figure 1. Electronic collimation. The schematic drawing represents the reconstruction of a point gamma source. Cones are determined from the interaction positions in both detectors and the measured energy of the scattered electron.

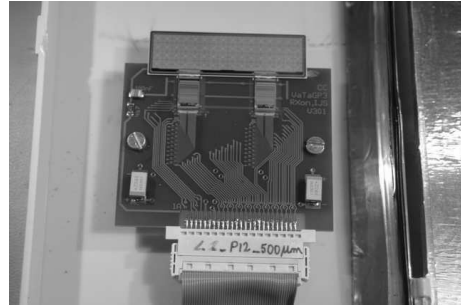


Figure 2. Photograph of a silicon module. A 500 μm thick, 256-pad silicon sensor(top) is bonded to a set of two VATAGP3 ASICs. The hybrid measures $5.9 \times 4.8 \text{ cm}^2$ and the sensor $4.5 \times 1.1 \text{ cm}^2$.

the pad and is DC coupled to the p^+ -doped implant, while the second metal layer routes the signals to the detector edge. Reverse bias is used to operate the sensor. A full depletion voltage of 110 V was inferred from C-V characteristics, while the I-V characteristic showed a current at that voltage of not more than 100 pA/pad.

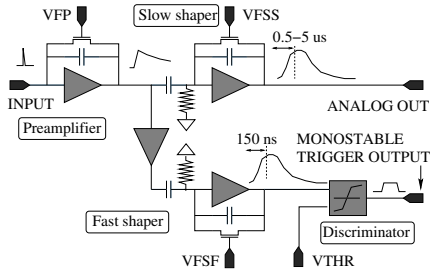


Figure 3. Approximate schematic of one of the 128 channels of a VATAGP3 ASIC.

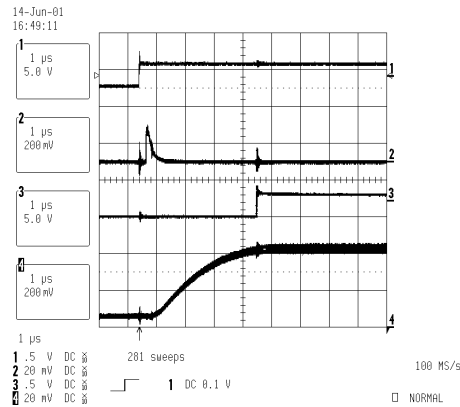


Figure 4. Oscilloscope screen-shot of the ASIC output. Charge injection simulating a Compton event (line 1) is followed by the monostable output of the discriminator(line 2). A 'hold' signal fixes the analog outputs, as shown in line 3. The output of the slow shaper, with shaping time of 4 μs , is shown in line 4. The output signal is latched near its maximum by the hold signal.

The VATAGP3, an ASIC produced by IDEAS [6], is used for recording the detector signals. Figure 3 shows a schematic of one of the 128 channels, while

figure 4 shows the output as seen on an oscilloscope. Each channel hosts a pre-amplifier and two shapers. The fast shaped signal (TA), with fixed shaping time of 150 ns, is discriminated to provide a monostable trigger signal (figure 4, line 2). The slow shaper (VA) has an adjustable shaping time of 0.5 - 5 μ s to provide a low-noise analog output (figure 4, line 4). A delayed 'hold' signal fixes the value of a channel during read-out (figure 4, line 3).

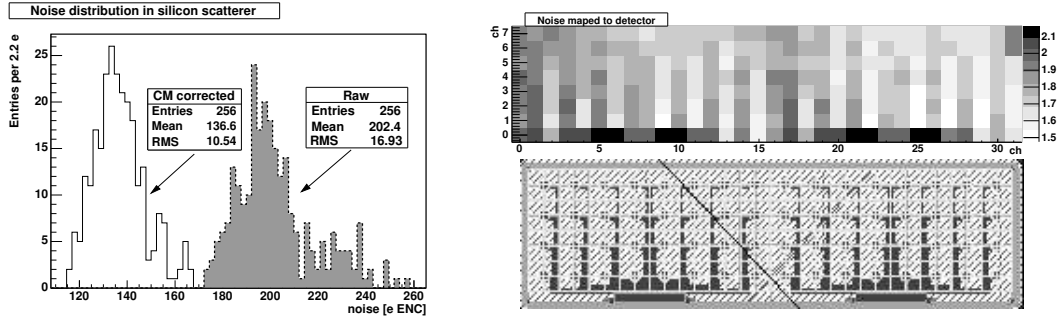


Figure 5. Left: Distribution of the noise of the slow shaper over the detector pads, with and without subtraction of the common mode (CM) noise. Right top: The noise mapped to the detector. Right bottom: Design of the detector.

The noise properties of the slow and fast shaper amplifiers were studied. First, the slow shaper was calibrated using γ -rays of ^{241}Am and ^{57}Co sources. The variance of the analog output of a given pad when no charge is present is an estimate of the read-out channel's noise. The distribution of the noise with/without correction for the common mode component is shown in figure 5. The noise of individual pads was mapped to the position on the detector. A comparison with the detector design shows that the read-out channels with higher noise correspond to pads with higher capacitance due to the routing on the second metal layer. The average variance of the equivalent noise charge (ENC) of a single pad is 137 e, which corresponds to energy resolution of 1.15 keV FWHM.

The fast shaped pulse can be observed at the input of the discriminator using a special probe pad. 60 keV photons from ^{241}Am gave the pulse shape shown in figure 6 (shaping time is $\tau = 150$ ns). Based on the baseline fluctuation, a noise of $\sigma_V = 620$ e ENC was estimated. Time-walk and jitter were tested with fixed charge injection into the preamplifier of the ASIC. The time walk for thresholds varying from 20% to 90% of the input pulse height was estimated at 130 ns. The jitter F_t (FWHM) due to the base line fluctuations can be estimated as $F_t = 2.35 \times \tau \sigma_V / A$, with A the signal amplitude. A charge injection of 6.8 fC gives $F_t = 5.2$ ns which is much smaller than the measured value of 12 ns. This could be attributed to the residual electronics jitter and the pulser instability.

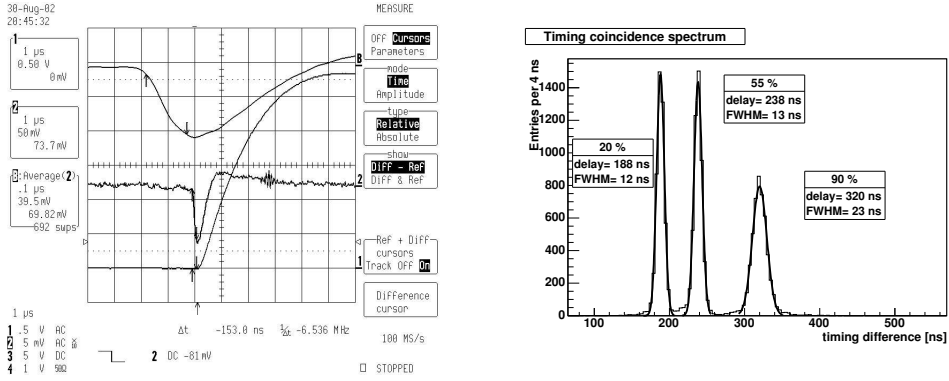


Figure 6. Left: The fast shaper output at the input of the discriminator. From the top: Averaged output of the fast shaper on a ten-fold magnified time scale (line B), and a single output of the fast shaper (line 2) compared to the slow shaped output (line 1). Right: Delay of the monostable trigger output, with fixed charge injection, for discriminator thresholds corresponding to 20 %, 55 % and 90 % of the input pulse height.

3 The scintillator module

The scintillator module, shown in figure 7, was taken from the SPRINT set-up [7]. A single head of the ring is composed of 44 NaI bars, which are 4 mm wide, 13 mm deep and 15 cm long, hence giving sensitive volume of $15 \times 17.6 \times 1.3 \text{ cm}^3$. The crystals are viewed by 20 Hamamatsu R980 photomultiplier tubes (PMT) with 3.8 cm diameter. Each PMT anode is biased to +1 kV with respect to the photo-cathode at ground potential and read out through a capacitor. The signals are amplified and shaped with a shaping time of 500 ns which matches the light collection time in the crystal. The sum of signals (energy sum) from all 20 PMT is obtained at the output of a summing amplifier.

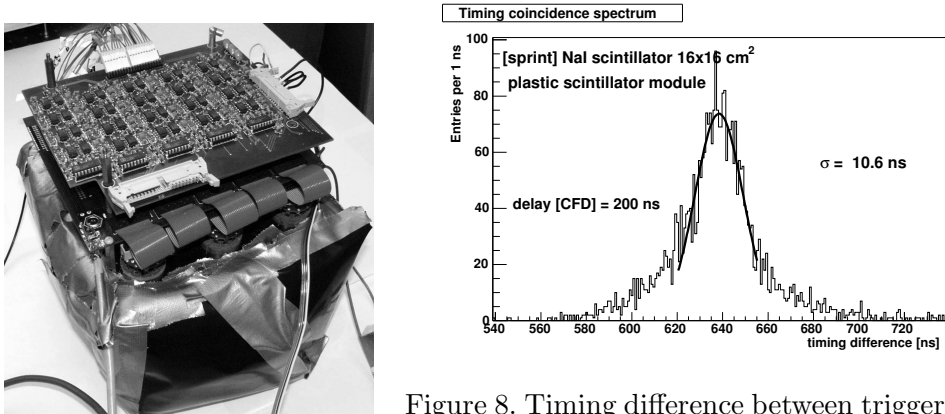


Figure 7. Photo of a SPRINT head.

Figure 8. Timing difference between triggers of the SPRINT module and a plastic scintillator. Coincidences of two back-to-back 511 keV photons emitted by ^{22}Na positron source.

The energy sum signal, fed into a constant fraction discriminator (CFD), was used for a trigger. The timing properties were tested with a ^{22}Na positron

source emitting two back-to-back 511 keV annihilation photons. One of the photons was captured by a fast plastic scintillator with anode output coupled directly to the CFD, giving a good timing reference. The timing difference of interactions in both scintillators, shown in figure 8, corresponds to a timing resolution of 25 ns FWHM.

4 Coincident setup

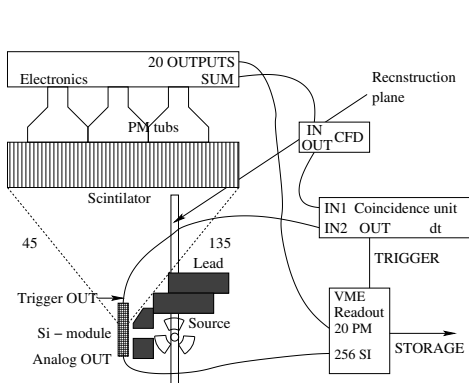


Figure 9. Schematic drawing of the coincidence set-up.

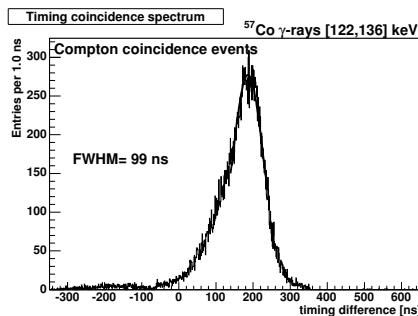


Figure 10. Timing difference of triggers from the SPRINT energy sum CFD and triggers from the silicon module for Compton scattered ^{57}Co photons and random background.

Both detectors were combined in a set-up as sketched in figure 9. The scatterer was fixed 12 cm below the absorber along its symmetry axis to allow for detection of photons with scattering angles between 45 and 135 degrees. Lead shielding was used to decrease the rate of direct hits in the absorber and to provide source collimation. To simulate the ^{99m}Tc source used in SPECT, a ^{57}Co source with activity of 150 was used which has two principal γ lines at 122 and 136 keV and almost negligible contribution from other lines. Figure 10 shows the timing difference between the silicon trigger (TA) and the trigger from the CFD on the energy sum for the ^{57}Co source. The distribution shows a clear peak for the Compton scattered photons and is asymmetric with a tail toward smaller delays, where the lower signals in the scatterer were recorded. This is a direct consequence of the time-walk of the silicon module, giving poor resolution of 99 ns FWHM. A coincidence window capturing 95 % of coincidences ($\pm 2\sigma$) is 200 ns long. No random coincidences can be seen in figure 10 so they represent a negligible contribution to the total coincidence rate of 50 Hz.

Events in the scatterer were recorded either in self-triggering mode or with coincidences. The spectra recorded in both cases are given in figure 11. The discriminator trigger level was at 8.2 keV, which enabled us to see Compton scattered events below the Compton edges at 39.4 and 47.2 keV. The coin-

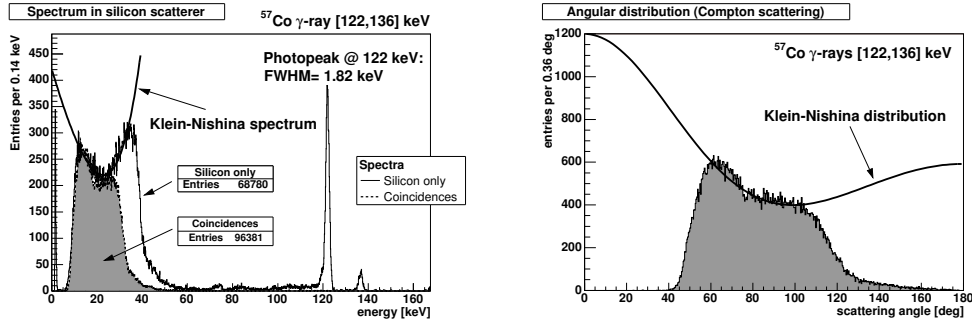


Figure 11. Scatterer results. Left: Energy spectra of photo-electrons recorded with coincidences or in self-triggering mode. Right: Angular distribution derived from the energy spectrum. Cross-sections were calculated using the Klein-Nishina formula and scaled to match the data.

coincidence energy spectrum shows only Compton scattered events, which agrees well with the negligible random coincidence rate obtained with the timing measurements. The measured data are consistent with the Klein-Nishina spectrum. Figure 11 also shows the scattering angle distribution, calculated from the scattered electron energy, conforming nicely to the Klein-Nishina prediction. Events fall in the range constrained by the setup geometry (figure 9). The scattering angle corresponding to the threshold energy is 45° , which imposes no further constraints.

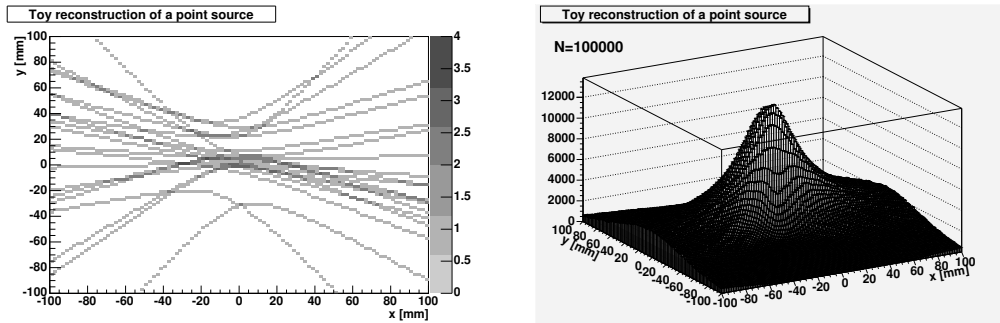


Figure 12. 'Toy' reconstruction of the source position on the reconstruction plane. Left: after $N=10$ events. Right: after $N=100000$ events.

Coincident data were used to perform a simple, 'toy' reconstruction. The intersections of a plane with the Compton-scattered cones were drawn for a fixed reconstruction plane (figure 9) containing the point source, parallel to the silicon detector and orthogonal to the scintillator crystal. The first ten ellipses/hyperbolas are shown on the left histogram of figure 12. After overlaying 100000 events, the histogram on the right is obtained, showing the approximate position of the source. The result confirms that the correct events are matched and Compton collimation is possible.

For a clinical imaging prototype several layers of silicon will be stacked to increase efficiency of the scatterer. Also a full scintillator ring will be employed to detect all scattered photons with a suitable scattering angle. This prototype

will be constructed in the middle of 2004.

5 Practical applications

A prostate probe is aimed at non-invasive screening of prostate cancer in men. Radio-tracers that accumulate in the malign tissue are available, but due to the low resolution of the existing SPECT detection methods no positive cancer identification is possible. The envisaged probe consists of a densely packed silicon array as the scatterer, inserted intra-rectally, and a scintillator-PM absorber surrounding the patient's body, as sketched in figure 13. Simulations [8] show a possible simultaneous 20-fold increase in efficiency and 5-fold improvement in spatial resolution compared to currently used gamma cameras based on mechanical collimation.

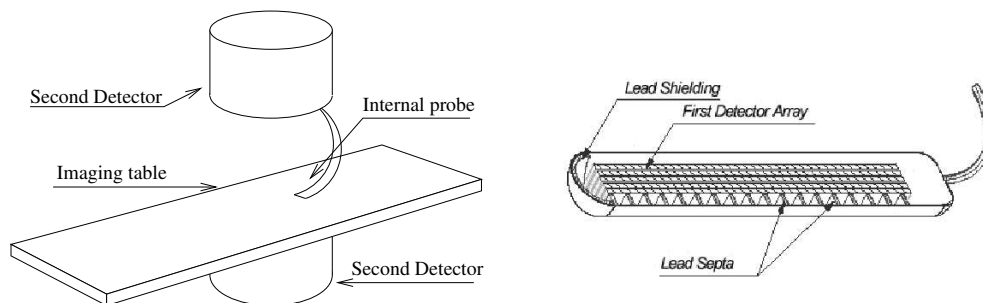


Figure 13. Drawing of the envisaged prostate probe. Left: External detector (scintillator-PM module) and a patient table. Right: Internal probe – densely packed scatterer array of silicon with lead shielding.

6 Summary

A crude Compton camera prototype was constructed using a pad silicon detector module coupled to a scintillation camera. The energy resolution of the silicon detector was measured at be 1.15 keV FWHM, close to the design value. Compton events from a ^{57}Co γ -ray source were observed. A 'toy' reconstruction successfully located the position of a point source, proving the principle of Compton scatter based collimation. Further studies will include several layers of silicon detectors and a full scintillator ring to increase efficiency of the set-up. The timing resolution will be improved using time-walk compensation for the scatterer trigger and a separate dynode output for the PMT module. More precise three-dimensional reconstruction algorithms will be employed for proper source distribution imaging.

Acknowledgements

One of us, A.C.M. acknowledges support from project **POCTI/FNU/49503/2002**, FCT Portugal. Also N.H.C, L.H., S.J.P., W.L.R, S.J.W. and L.Z would like to acknowledge support from the US DHHS National Institutes of Health grants **R01 EB000430-22** and **R33 EB002186-04**.

References

- [1] R. W. Todd, J. M. Nightingale, and D. B. Everett. “A Proposed gamma-Camera”. *Nature*, **251** (1974) 132.
- [2] P. Weilhammer *et al.* “Si Pad Detectors”. *Nucl. Instr. Meth.*, **383** (1996) 89-97.
- [3] D. Meier, A. Czermak, P. Jalocha, M. Kowal, B. Sowicki, W. Dulinski, et al. “Silicon Detector for a Compton Camera in Nuclear Medical Imaging”. *IEEE Trans. Nucl. Sci.*, **49** (2002) 812-6.
- [4] A. Studen, V. Cindro, N. H. Clinthorne, A. Czermak, W. Dulinski, J. Fuster, et al. Development of silicon pad detectors and readout electronics for a compton camera. *Nucl. Inst. Meth. A*, **501** (2003) 273-9.
- [5] SINTEF. Foundation of Scientific and Industrial Research at the Norwegian Institute of Technology, Electronics and Cybernetics, Microsystems. <http://www.oslo.sintef.no/ecy/>. Oslo and Trondheim, Norway.
- [6] Integrated Detector and Electronics (IDE) AS. <http://www.ideas.no>. Pb.315, Veritasveien 9, N-1322 Høvik, Norway, Tel: ++47-6755-1818.
- [7] J.W. LeBlanc. “C-SPRINT: A Prototype Compton Camera System for low Energy Gamma Ray Imaging”. *IEEE, Trans. Nucl. Sci.*, **45** (1998) 3.
- [8] L. Zhang. “An Innovative High Efficiency and High Resolution Probe for Prostate Imaging”. *Journal of Nuclear Medicine*, **41** (2001) 4, Suppl.